BCL-x_L-Dependent Light Scattering by Apoptotic Cells

Nada N. Boustany,* Yien-Che Tsai,† Bryan Pfister,‡ Wilsaan M. Joiner,§ George A. Oyler,¶‖ and Nitish V. Thakor§

*Department of Biomedical Engineering, Rutgers University, Piscataway, New Jersey 08854; †Laboratory of Protein Dynamics and Signaling, National Cancer Institute, Frederick, Maryland; ‡Department of Neurosurgery, University of Pennsylvania School of Medicine, Philadelphia, Pennsylvania; §Department of Biomedical Engineering, Johns Hopkins University, Baltimore, Maryland; ¶Department of Neurology, University of Maryland School of Medicine, Baltimore, Maryland; and ‖Research Services, Baltimore VA Medical Center, Baltimore, Maryland

ABSTRACT We measured the intensity ratio of wide-to-narrow angle scatter, optical scatter image ratio (OSIR), in single cells during apoptosis and after overexpression of the mitochondria-bound antiapoptotic protein BCL-x_L. OSIR is sensitive to particle size/shape for objects with wavelength-scale dimensions, and was used as a morphometric measure of cellular response. Three cell variants were treated with staurosporine (STS): nontransfected parental CSM14.1, CSM14.1 stably expressing yellow fluorescent protein (YFP) with diffuse YFP fluorescence, and apoptosis-resistant CSM14.1 stably expressing the fusion protein construct YFP-BCL-x_L with YFP fluorescence localized on the mitochondria. After treatment with 1 or 2 μM STS, the measured OSIR decreased monotonically by $\sim$25% in the nontransfected and YFP variants, and reached a steady-state value 40–60 min after STS treatment. The decrease in OSIR at the onset of apoptosis preceded phosphatidyl serine exposure by 5 h. In the YFP-BCL-x_L cell variant, the initial OSIR was already $\sim$24% lower than the initial OSIR in YFP and nontransfected cells, and only decreased by $<$10% after STS treatment. Alterations in light scattering by cells overexpressing BCL-x_L even before apoptosis induction raise interesting questions as to the role of BCL-x_L in conferring apoptosis resistance by preconditioning the cells and possibly altering mitochondrial morphology.

INTRODUCTION

Programmed cell death (apoptosis) is a highly regulated form of cell death fundamental to normal tissue development and homeostasis. Apoptosis is characterized by a number of well-defined molecular events shown in many cases to converge on mitochondria (Desagher and Martinou, 2000; Gross et al., 1999). In these cases, initiation of apoptosis leads to the release of cytochrome *c* from the mitochondrial intermembrane space. The release of cytochrome *c* into the cytoplasm results in the activation of intracellular proteases, caspases, which eventually induce nuclear and DNA fragmentation, and breakdown of subcellular structure. Cytochrome *c* release from the mitochondria is controlled by the activity of proteins of the BCL-2 family, such as the proapoptotic proteins Bax, Bak, Bid, Bad, and the antiapoptotic proteins BCL-2 and BCL-x_L (Gross et al., 1999). The actual mechanism by which cytochrome *c* is released from the mitochondria is still under debate.

To investigate the role of mitochondrial morphology in apoptosis, single-angle light-scattering data (90° or forward scatter) (Narita et al., 1998; Vander-Heiden et al., 1997), and absorption spectrophotometry (Finucane et al., 1999; Jurgensmeier et al., 1998; Ott et al., 2002; Zamzami et al., 1996) have been used to detect volume changes in suspensions of viable mitochondria isolated from apoptotic cells. Different results were obtained with these techniques, with some studies showing light scattering suggestive of mitochondrial swelling (Narita et al., 1998; Vander-Heiden et al., 1997; Zamzami et al., 1996), whereas others showed no change in light scattering indicating no mitochondrial swelling (Finucane et al., 1999; Jurgensmeier et al., 1998; Ott et al., 2002). Electron microscopy has been used to directly assess mitochondrial matrix morphology in fixed samples, and has led to several findings including: 1), swelling and outer membrane rupture (Vander-Heiden et al., 1997); 2), reduction in mitochondrial size (Mancini et al., 1997; Martinou et al., 1999); 3), preservation of mitochondrial structure (von Ahsen et al., 2000); 4), mitochondrial blebbing (Mootha et al., 2001); 5), mitochondrial fission (Frank et al., 2001); 6), mitochondrial proliferation (Camilleri-Broet et al., 1998; Mancini et al., 1997; Reipert et al., 1995); and 7), remodeling of the cristae (Scorrano et al., 2002).

Recent data have also shown that proteins of the BCL-2 family may be directly involved in altering mitochondrial morphology. For example, studies by Kowaltowski et al. (2002) showed that BCL-2, an antiapoptotic protein partially localized to the mitochondrial membrane, induces a change in the size and complexity of isolated mitochondria as measured by flow cytometry, whereas studies by Scorrano et al. (2002) showed that the proapoptotic protein t-Bid induces matrix remodeling upon its translocation to the outer membrane of isolated mitochondria as evidenced by electron tomography.

In this report, we investigate whether apoptosis or overexpression of BCL-x_L will result in detectable alterations in light scattering that can be measured in real time

Submitted June 29, 2004, and accepted for publication September 3, 2004.

Address reprint requests to N. N. Boustany, PhD, Dept. of Biomedical Engineering, Rutgers University, 617 Bowser Rd., Piscataway, NJ 08854. Tel.: 732-445-5337; Fax: 732-445-3753; E-mail: nboustan@rci.rutgers.edu.

0006-3495/04/12/4163/09 $2.00

doi: 10.1529/biophysj.104.048736

within monolayers of live cells in culture. To this end, we use a microscopy technique we recently developed, optical scatter imaging, capable of measuring light scattering directly within subcellular compartments of cultured cells (Boustany et al., 2002, 2001). The technique consists of measuring the intensity ratio of wide-to-narrow angle scatter, optical scatter image ratio (OSIR), at every pixel bin of a microscopic image. This technique allows for real-time tracking of morphological changes in situ and is sensitive to changes in size/shape of objects with wavelength-scale dimensions. Recently, we showed that an increase in the scatter-intensity ratio was correlated with mitochondrial rounding in response to an increase in intracellular calcium (Boustany et al., 2002). In this report we show that intracellular changes in angular light scattering can be detected within the first 60 min of apoptosis, several hours before phosphatidyl serine exposure, or loss of plasma membrane integrity. We also show that these light-scattering changes are modulated by the overexpression of mitochondria-bound BCL-x_L.

METHODS

Molecular biology and generation of cell lines

Mouse BCL-x_L (kindly provided by J. M. Hardwick at Johns Hopkins University) was cloned into the enhanced yellow fluorescent protein (EYFP)-C1 vector (Clontech, BD Biosciences, Palo Alto, CA) using the *Bgl*II restriction site to yield a plasmid encoding a yellow fluorescent protein (YFP) fused to BCL-x_L protein. CSM14.1 cells cultured in 100-mm dishes (50% confluence) were transfected with an empty plasmid encoding hygromycin resistance and either YFP or YFP-BCL-x_L (1:10 molar ratio, hygromycin plasmid/fluorescent protein plasmid) using lipofectamine (Invitrogen, Carlsbad, CA). After 24 h, cells were cultured in medium supplemented with 1 mg/ml G418-sulfate and 400 μg/ml hygromycin. Isolated foci were selected for expansion. Cells expressing the highest-level fluorescence (10th percentile) were sorted by fluorescence-activated cell sorting, diluted, and replated in 96-well plates to obtain clonal cell lines. Expression of YFP or YFP-BCL-x_L in cell lines were confirmed by immunoblots (see Fig. 1).

Immunoblots

Parental CSM14.1 cells and cells stably expressing YFP or YFP-BCL-x_L were lysed in lysis buffer (38 mM NaCl, 10 mM HEPES, pH = 7.4, 2 μM leupeptin, 0.15 μM aprotinin, 0.2 mM PMSF, 2% SDS) and briefly sonicated. Equal amounts of protein were resolved by SDS-PAGE, transferred to nitrocellulose membranes, incubated with the appropriate antibodies, and visualized by chemiluminescence. YFP was detected with mouse anti-GFP antibody (0.2 μg/ml; catalog no. SC-9996, Santa Cruz Biotech, Santa Cruz, CA); BCL-x_L with mouse monoclonal anti-BCL-x_L (2 μg/ml; catalog no. 556499, BD Pharmingen, San Diego, CA).

Cell culture

CSM 14.1 cells were maintained in Dulbecco's modified Eagle's medium (DMEM) supplemented with 10% fetal bovine serum (FBS), 100 units/ml penicillin, and 100 μg/ml streptomycin (DMEM, FBS, penicillin and streptomycin from Invitrogen). The cells were kept in culture at 29°C in a 5% CO2 in air atmosphere. For microscopy, cells were cultured on glass coverslips coated with poly-D lysine (molecular weight of >300,000; Sigma Chemical, St. Louis, MO).

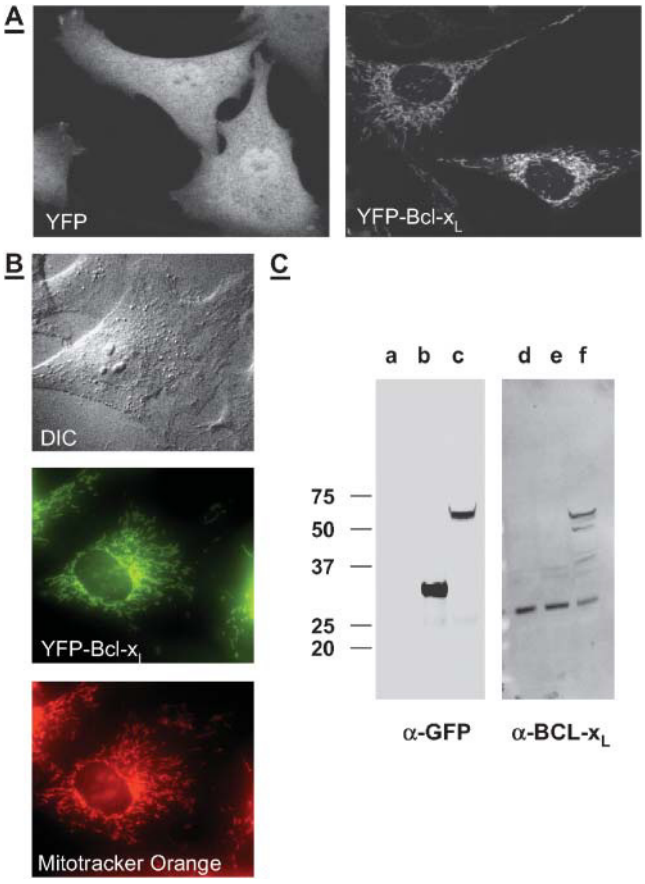

FIGURE 1 YFP and YFP-BCL-x_L expression in CSM 14.1 cell lines. (*A*) Distribution of YFP fluorescence in cell lines transfected with YFP (*left*) and YFP-BCL-x_L (*right*). (*B*) Differential interference contrast (DIC; *top*) and fluorescent images of a cell transfected with YFP-BCL-x_L. The distribution of YFP-BCL-x_L (*middle*) coincides with the distribution of Mitotracker Orange (*bottom*), and is restricted to the mitochondria. (*C*) Expression of YFP and YFP-BCL-x_L is confirmed by Western blots. Equal amount of lysates of nontransfected cells (lanes *a* and *d*), cells stably expressing YFP (lanes *b* and *e*), or YFP-BCL-x_L (lanes *c* and *f*) were immunoblotted for YFP (*left*) or BCL-x_L (*right*).

Apoptosis experiments

Each coverslip with attached live cells was mounted by means of a steel plate onto the stage of the inverted microscope. Just before mounting onto the microscope's stage, the DMEM growth medium was replaced with Leibovitz L15 growth medium (Invitrogen) supplemented with 10% fetal bovine serum, 100 units/ml penicillin, and 100 μg/ml streptomycin). With the cells on the microscope stage, apoptosis was induced by replacing the L15 growth medium with the same supplemented with 1 μM or 2 μM staurosporine (Sigma Chemical) prepared from a 4-mM stock solution of staurosporine (STS) in DMSO. The cells were monitored by differential interference contrast, fluorescence, and optical scatter imaging microscopy at room temperature and room air. Treatment with DMSO was used as a negative control. The two DMSO concentrations equivalent to those used in the cases of 1 μM and 2 μM STS, respectively, yielded similar results, which were pooled.

Apoptosis assays

To assess whether the cells treated with STS were undergoing apoptosis, CSM14.1 cells were exposed to 1 μM STS and analyzed at different time points up to 48 h. Standard fluorescence assays based on Annexin V binding, propidium iodide, and TdT-mediated dUTP nick end labeling (TUNEL) were utilized to detect phosphatidyl serine flipping and extracellular exposure, loss of membrane integrity, and DNA fragmentation, respectively. Apoptosis was also confirmed by the positive observation of typical apoptotic morphological features consisting of cell shrinkage, formation of apoptotic bodies, and nuclear fragmentation. Annexin V, propidium iodide, and TUNEL assay kits (Roche, Indianapolis, IN) were used according to the manufacturer's protocols.

Fluorescence microscopy

Labeled cells were observed in situ either on the optical scatter imaging microscope platform, which was also fitted with an epiflorescence modality, or separately (Fig. 1 *A*) on a confocal microscope (LSM 510, Zeiss, Jena Germany). In selected cases, the live nontransfected CSM 14.1 variants were prelabeled with the fluorescent mitochondrial probe Mitotracker Green or Mitotracker Orange (Molecular Probes, Eugene, OR) to visualize specifically the mitochondria. For this, the cells were incubated for 45 min in growth medium supplemented with 100 nM Mitotracker Green or 200 nM Mitotracker Orange at 29°C in the 5% CO_2 in air atmosphere, before transferring the coverslips to the microscopy setup. Mitotracker Green and Annexin V were observed with an EN GFP-LP filter cube (catalog no. 41018, Chroma Technology, Brattleboro, VT) with the following specification: excitation band-pass filter, 470 ± 20 nm; emission filters, >495 nm long pass followed by another >500 nm long pass. Mitotracker Orange, propidium iodide, and TUNEL staining were observed with a standard ''TRITC'' (rhodamine) filter cube (catalog no. G-2E/C, Nikon, Melville, NY): excitation band-pass filter, 540 ± 12.5 nm; emission filters, >565 nm long pass followed by a 605 ± 27.5-nm band-pass filter. For nonconfocal imaging of the YFP-labeled cells, we used a custom-made filter cube (Chroma Technology): excitation band-pass filter, 500 ± 15 nm; emission filters, >530 nm long pass followed by a 545 ± 15 nm band-pass filter. For confocal imaging of YFP, the excitation source was a krypton/argon laser emission at 488 nm used with a 500–550 nm emission band-pass filter.

Light scatter microscopy

The optical scatter imaging technique was described previously in detail (Boustany et al., 2002, 2001). The specimens were mounted on the stage of an inverted microscope (Eclipse T300, Nikon) with epifluorescence and differential interference contrast (DIC) imaging capabilities. The condenser numerical aperture (NA) was adjusted to 0.03 (condenser front aperture closed). A 10-nm band-pass interference filter placed in the condenser housing yielded an incident red beam centered at $\lambda = 630$ nm. The images were collected with a 60× oil immersion objective, 1.4 NA, and displayed on a charge-coupled device camera (Sensicam, Cooke, Auburn Hills, MI). In a Fourier plane conjugate to the back focal plane of the objective, a beam stop was placed in the center of an iris with variable diameter. The iris diameter was set in either a low NA, or a high NA position. The variable iris collected light scattered within a solid angle, bound by $2° < \theta < 10°$ for low NA, and $2° < \theta < 67°$ for high NA.

Data acquisition and image analysis

For each specimen studied, two sequential dark-field images, collected 20–30 s apart, were acquired at high and low NA by manually switching the diameter of the variable iris between high and low NA. A sample consisting of the L15 growth medium served to provide the background-scatter signal due to the microscope optics. This background signal was subtracted from each image. The background-subtracted dark-field images were binned into pixels, where each pixel is the image of a 1.6×1.6 μm^2 object area. Dividing the background-subtracted high NA image by its corresponding background-subtracted low NA image resulted in ratiometric optical scatter images, which directly encode the high-to-low NA optical scatter intensity ratio at each pixel bin in the field of view.

The OSIR corresponds to the intensity scatter ratio of wide-to-narrow angle scatter defined as:

$$OSIR = \frac{\int_{\phi=0}^{360°}\int_{\theta=2°}^{67°} F(\theta,\phi)\sin\theta\, d\theta\, d\phi}{\int_{\phi=0}^{360°}\int_{\theta=2°}^{10°} F(\theta,\phi)\sin\theta\, d\theta\, d\phi}, \quad (1)$$

where $F(\theta,\phi)$ gives the intensity of the light scattered in a given direction defined by the angles θ and ϕ. θ is the angle between the scatter direction and the direction of propagation of the incident light, and ϕ is the azimuthal angle of scatter. For spheres with diameter between 0.3 and 3 μm, and with refractive index ratio $m \sim 1$, the OSIR decreases nonlinearly and monotonically from a value of 20 to a value of 1.15 as a function of sphere diameter (Boustany et al., 2001). For sphere diameters >3 μm, the OSIR oscillates very slowly around a constant value and remains under 1.5.

In each experiment, a segment region was initially defined around every cell using the DIC images. These segments were then overlaid onto the optical scatter images such that data analysis was limited to regions that contained a cell. Only pixels with $OSIR \geq 1.15$ were considered at any time point to exclude pixel values outside the measurement's theoretical dynamic range. Optical scatter images were acquired in IPlab (Scanalytics, Fairfax, VA) and processed in Matlab (The Math Works, Natick, MA).

RESULTS

YFP expression in CSM 14.1 cells

CSM 14.1 cells stably expressing yellow fluorescent protein exhibit a bright and diffuse green-yellow fluorescence throughout the whole cell (Fig. 1 *A*, *left*). Cells stably expressing YFP-BCL-x_L exhibit a bright green-yellow fluorescence with a filamentous distribution (Fig. 1 *A*, *right*). The distribution of YFP-BCL-x_L coincided with the distribution of mitochondria (compare colocalization of YFP and Mitotracker Orange fluorescence in Fig. 1 *B*, *middle* and *bottom*, respectively). The fluorescence image panels in Fig. 1 *B* were corrected for emission cross talk between the YFP and Mitotracker Orange channels. By observing cells labeled with either Mitotracker Orange or YFP-BCL-x_L in each fluorescence channel, the amount of cross talk was measured. We found that, for the same image acquisition time in each channel, the equivalent of 12% of Mitotracker Orange signal measured in the Mitotracker Orange channel overflows into the YFP channel, whereas the equivalent of only 1% of YFP signal measured in the YFP channel overflows into the Mitoctracker Orange channel. Expression of YFP and YFP-BCL-x_L were confirmed by immunoblots against YFP and BCL-x_L (Fig. 1 *C*). All cell variants expressed endogenous BCL-x_L (band between 25 and 37 kD in lanes *d–f* in Fig. 1 *C*). In addition, cells transfected with YFP-BCL-x_L exhibited a band between 50 and 75 kD corresponding to expression of the fusion construct YFP-BCL-x_L (lanes *c* and *f* in Fig. 1 *C*). Cells

transfected only with YFP exhibited a band between 25 and 37 kD corresponding to YFP expression (lane *b* in Fig. 1 *C*).

Effect of staurosporine on CSM 14.1 cells

When challenged with 1 μM or 2 μM STS, CSM14.1 cells exhibited the morphological hallmarks of apoptosis, including initial cell shrinkage, formation of apoptotic bodies, and nuclear fragmentation. In addition, the cells exhibited positive Annexin V binding, and positive propidium iodide and TUNEL staining. The onset of positive Annexin V binding occurred at 6 h, after which the percentage of positively fluorescent cells started rising steeply to reach 70% at 25 h (Fig. 2 *A*, *open circles*). The onset of positive nuclear propidium iodide labeling occurred at 10 h, with 45% of the cells exhibiting positive nuclear propidium iodide fluorescence at 25 h (Fig. 2 *A*, *solid diamonds*). By comparison at 25 h, 25% of cells treated with DMSO (negative control) stained positively for Annexin V, and 1.2% of cells treated with DMSO stained positively for propidium iodide (data not shown). The TUNEL assay was conducted up to 47 h, at which point 28% of the cells treated with 1 μM STS stained positively for TUNEL (Fig. 2 *A*, *shaded squares*), compared to 2% of the cells treated with DMSO (data not shown). Nuclear fragmentation was observed in positively TUNEL stained nuclei. The YFP-BCL-x_L variants were more resistant to cell death than their nontransfected and YFP counterparts (Fig. 2 *B*). The number of nonviable BCL-x_L cells was half that of the YFP cells 72 h after STS treatment, assayed by counting the fraction of propidium-iodide-labeled cells.

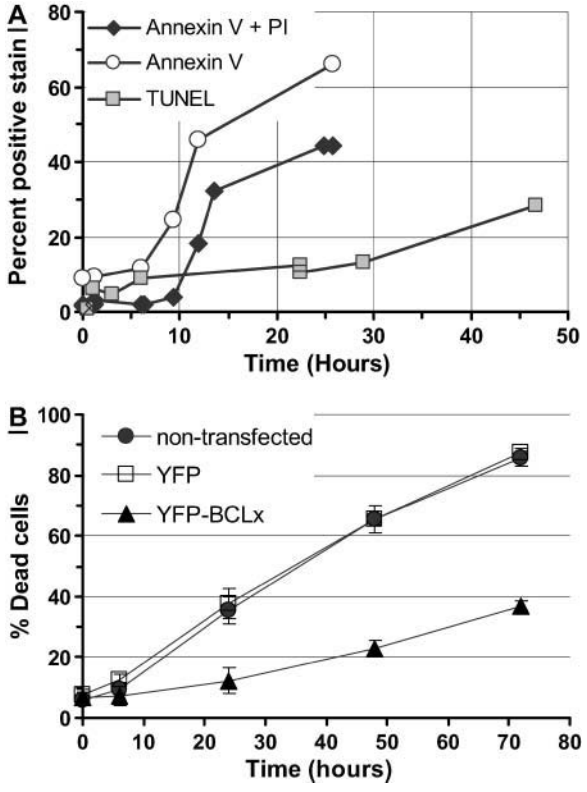

FIGURE 2 Apoptosis response to staurosporine (STS). (*A*) Time course showing the percentage of cells ($n > 990$ for each data point) exhibiting positive Annexin V fluorescence (*open circles*), positive Annexin V and propidium iodide fluorescence (*solid diamonds*), and positive TUNEL staining (*shaded squares*). (*B*) Time course showing the percentage of nonviable CSM14.1 cells ($n > 100$ for each point) assayed by propidium iodide after treatment with 1 μM STS. Solid circles, nontransfected; open squares, YFP; solid triangles, YFP-BCL-x_L.

Alterations in light scattering at onset of apoptosis

To investigate subcellular changes in light scatter at the onset of apoptosis, CSM14.1 cells were treated with 1 μM or 2 μM STS, and the OSIR was monitored over time. Fig. 3 *A* shows typical light-scattering changes in a CSM 14.1 cell during the first hour of STS treatment. The cell was also labeled with the fluorescent mitochondrial probe, Mitotracker Green. In the optical scatter images, the pixel intensity corresponds to the value of the $OSIR \times 10^2$, where the OSIR is defined in Eq. 1. The optical scatter images show a 36% decrease in the average OSIR (average pixel value) from 2.5 to 1.6 in this cell (Fig. 3 *B*). The OSIR decrease was monotonic and reached a steady-state value between 40 and 60 min after treatment. The OSIR decrease was accompanied by overall cellular shrinkage. However, the OSIR decrease was not accompanied by well-defined intracellular changes in the DIC images, or by significant mitochondrial redistribution or remodeling that could be observed in the fluorescent images. The OSIR decrease during the first 60 min of staurosporine treatment was reproducible and was observed in 54 of all 59 nontransfected cells challenged with either 1 μM ($n = 29$) or 2 μM ($n = 30$) STS.

To quantify the change in pixel intensity, which corresponds to the change in OSIR, we examined the ensemble of pixel values in the optical scatter images of all the untransfected cells. We plotted the initial and final histograms of image pixel values at $t < 0$ and $t = 60$ min (Fig. 3 *C*) for all the cells treated with 2 μM STS, 1 μM STS, or DMSO. The OSIR values were binned into 0.1 OSIR intervals, and the histograms are shown for $1.15 \leq OSIR \leq 10.05$. More than 95% of the pixel values >1.15 were included in this range. The histograms were normalized to the number of pixels in the $OSIR = 1.15$ bin (first bin). After STS treatment, the distribution of the pixels became narrower with most of the pixels with OSIR values <3. After STS treatment, the change in these optical scatter image histograms was characterized by a 26% decrease in the average pixel value (average OSIR) from 1.85 to 1.37 in the case of 1 μM STS and 21% in the case of 2 μM STS (Fig. 3 *D*), from 1.84 to 1.46. The monotonic decrease in mean pixel value (Fig. 3 *D*) mirrored the monotonic decrease in average OSIR signal observed in the individual cells (Fig. 3 *B*). In the cells treated only with

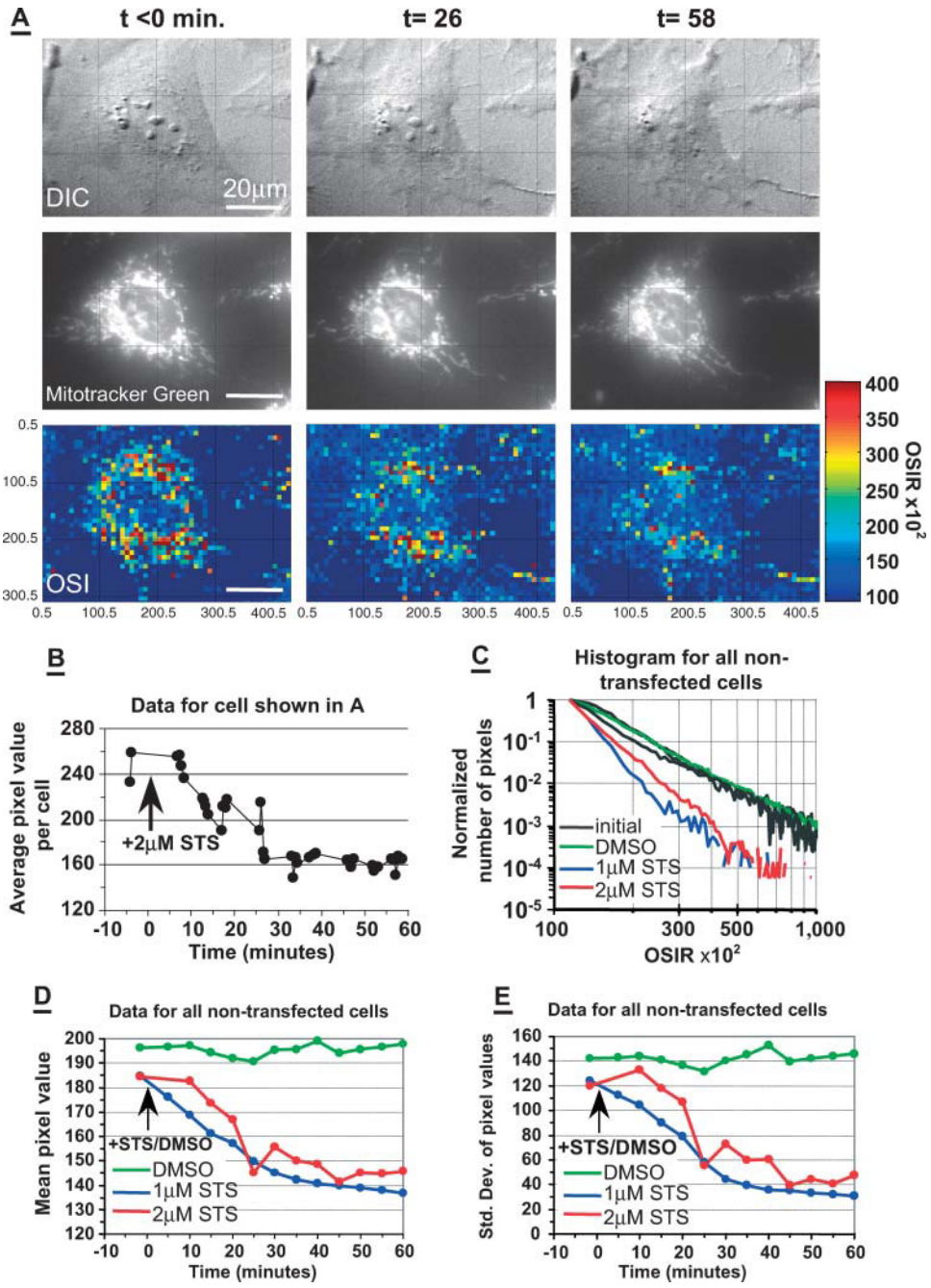

FIGURE 3 Light scattering response to STS. (*A*) Sequential images of a nontransfected, Mitotracker-labeled, CSM 14.1 cell before and after treatment with 2 μM STS at $t = 0$. Top panels, DIC; middle panels, Mitotracker Green fluorescence; bottom panels, optical scatter images (*OSI*) with pixel intensity equal to OSIRx10^2 (OSIR defined in Eq. 1). (*B*) Average OSIR measured in the cell shown in panel *A* and plotted as a function of time. (*C*) Normalized histogram of pixel values collected in all image segments of nontransfected cells before treatment (initial; *black solid lines*), and after treatment with DMSO (*green solid line*, 75 cells), 1 μM STS (*blue solid line*, 29 cells) or 2 μM STS (*red solid line*, 30 cells). Each of the initial black solid lines corresponds to each of the three groups of cells later treated with DMSO, 1 μM STS, or 2 μM STS. (*D*) Histogram means calculated before normalization of histogram, and plotted as a function of time. (*E*) Histogram standard deviations calculated before histogram normalization, and plotted as a function of time. In panels *D* and *E*, the data were averaged over 5-min time intervals.

DMSO there was no monotonic OSIR decrease. The narrowing of the pixel distribution was reflected by the decrease in the standard deviation of the pixel values as time progressed after STS treatment (Fig. 3 *E*).

Modulation of light scatter by overexpression of BCL-x_L

We investigated if the OSIR decrease could be modulated or stopped by the overexpression of the mitochondria-bound antiapoptosis protein BCL-x_L. Sample cells stably expressing YFP (Fig. 4) or YFP-BCL-x_L (Fig. 5) are depicted before and after STS treatment. Ensemble pixel values in images of cells overexpressing YFP or BCL-x_L were analyzed in Fig. 6. Fig. 6, *A* (YFP) and *B* (YFP-BCL-x_L), show the normalized initial histograms (*black lines*) and final histograms of pixel distributions after treatment with DMSO (*green lines*), 1 μM STS (*blue lines*), or 2 μM STS (*red lines*). Similarly to the nontransfected cells (Fig. 3), the distribution of pixel values in the YFP case became narrower and shifted to lower pixel values after STS treatment. In contrast, the initial pixel values in the BCL-x_L case start out

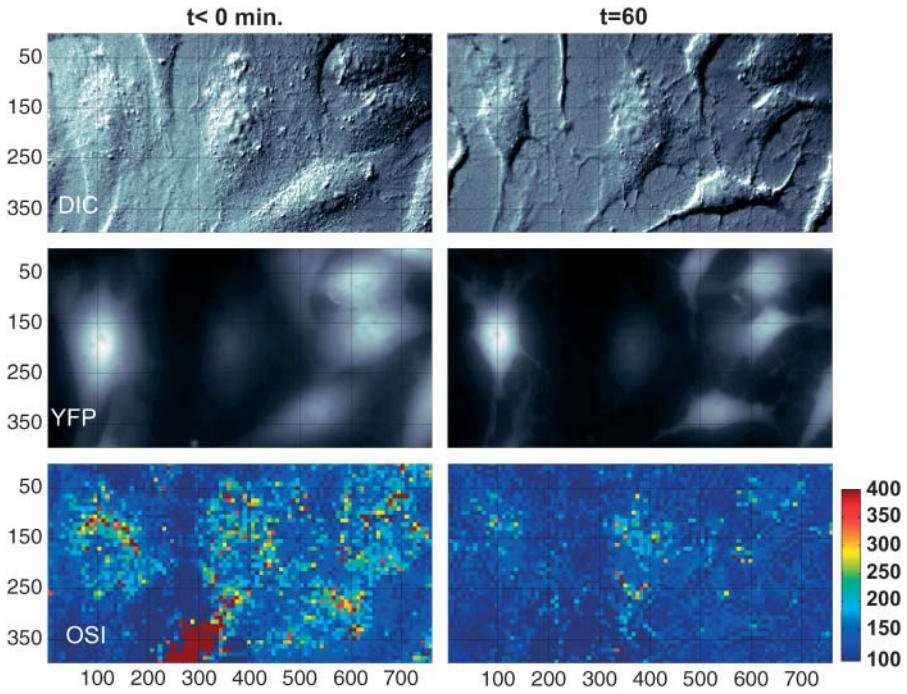

FIGURE 4 Partial field of view showing six YFP expressing cells before (*left panels*) and 60 min after (*right panels*) treatment with 2 μM STS at $t = 0$. Top panels, DIC; middle panels, YFP fluorescence; bottom panels, optical scatter images (*OSI*).

with a histogram, which is already very close to the final histogram at $t = 60$ min.

We compared change in mean pixel values (histogram means) over time for the three cell variants (Fig. 7 *A*). The altered initial histogram of the BCL-x_L pixel values, together with the preservation of the same final pixel value distribution as that observed in the YFP cells, ultimately resulted in a very small relative change in average OSIR (average pixel value) for the BCL-x_L cells: 8.8% decrease from 1.49 to 1.36 for BCL-x_L cells (1 μM STS) compared with a 28% decrease from 2.09 to 1.50 in the YFP case (1 μM STS). Although the BCL-x_L OSIR initial value is closer to the lower-bound OSIR value, $OSIR = 1.15$, the pixel values in the BCL-x_L case do remain above this minimum OSIR value, and are still within the theoretical dynamic range of the OSIR measurement.

Analysis of the histograms accounts for the changes in pixel intensity, where the pixel ensembles represent an ensemble of data points collected for each of the CSM cell variants in a given experimental condition. To assess the optical scatter response on a cell-by-cell basis, and the cellular variability in this response, we examined the scattering response on a single-cell basis by calculating the average OSIR for each cell segment in the nontransfected, YFP, and BCL-x_L cases. Fig. 7 *B* summarizes the average initial and final OSIR values calculated on a cell-by-cell basis for the different experimental

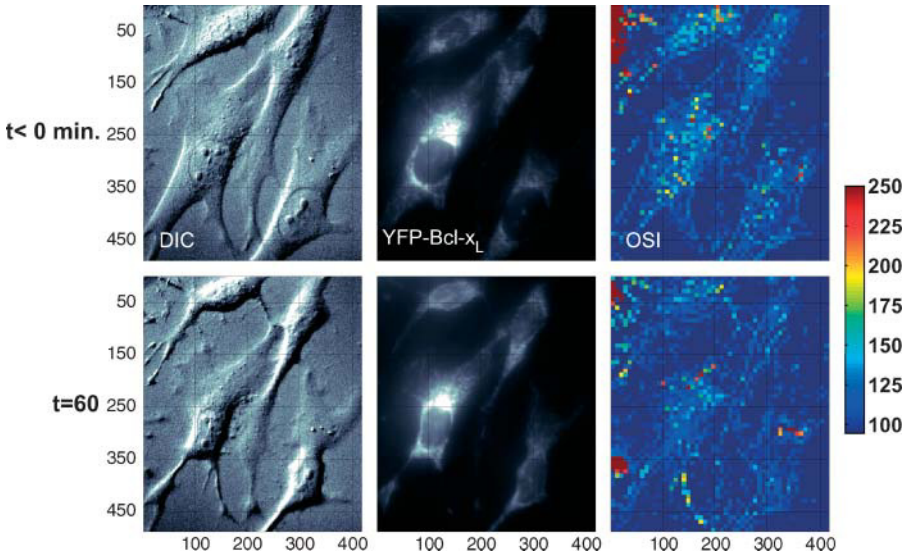

FIGURE 5 Partial field of view showing four YFP-Bcl-x_L transfected cells before (*top panels*) and 60 min after (*bottom panels*) treatment with 2 μM STS at $t = 0$. Left panels, DIC; middle panels, YFP fluorescence; right panels, optical scatter images (*OSI*).

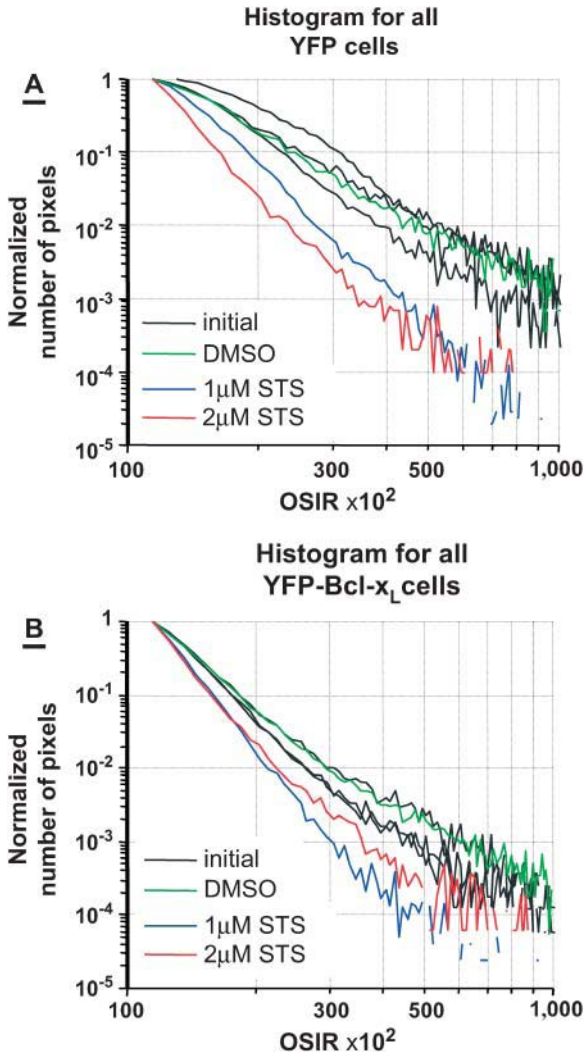

FIGURE 6 OSI pixel analysis for all YFP and YFP-BCL-x_L cells. (*A*) Normalized histogram of pixel values for YFP transfected cells before treatment (*initial*), and after treatment with DMSO (11 cells), 1 μM STS (100 cells), or 2 μM STS (40 cells). (*B*) Normalized histogram of pixel values for YFP-BCL-x_L transfected cells before treatment (*initial*) or after treatment with DMSO (68 cells), 1 μM STS (138 cells), or 2 μM STS (55 cells). Each of the three black solid lines corresponds to the initial histogram for each of the three groups of cells later treated with DMSO, 1 μM STS, or 2 μM STS.

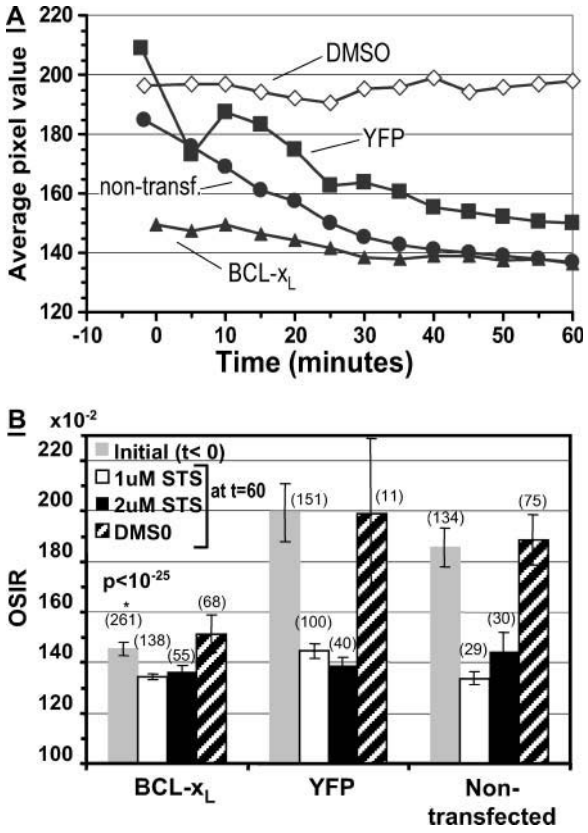

FIGURE 7 (*A*) Comparison of OSI pixel histogram mean for non-transfected cells (*solid circles*), YFP cells (*solid squares*), and BCL-x_L cells (*solid triangles*) treated with 1 μM STS at $t = 0$. Open diamonds, nontransfected cells treated with DMSO. Data averaged over 5-min time intervals. Pixel value = $OSIR \times 10^2$. (*B*) Average OSIR calculated on a single-cell basis before STS treatment (*shaded bar*), and 60 min after treatment with DMSO (*cross-hatched bar*), 1 μM STS (*open bar*), or 2 μM STS (*solid bar*). $P < 10^{-25}$ on the BCL-x_L shaded bar indicates a very low correlation probability between the initial populations of YFP and YFP-BCL-x_L transfected cells (Student's *t*-test). Error bars represent the 95% confidence interval of the mean. The number of cells tested in each case is in parentheses.

conditions. The single-cell analysis (Fig. 7 *B*) corroborates the analysis of image histograms (Figs. 3 and 6). In particular, we find that the average OSIR per cell is reduced after 60 min of apoptosis induction in YFP and nontransfected cells, and that the BCL-x_L cells start out with a significantly lower OSIR baseline value compared to their YFP counterparts ($p < 10^{-25}$ by Student's *t*-test; also compare initial optical scatter image (OSI) intensities in Figs. 4 and 5).

DISCUSSION

In an effort to continuously and noninvasively track the temporal sequence of subcellular morphological changes in situ, we have devised an optical method to observe alterations in angular light scatter by single living cells. Using this technique, we imaged the intensity ratio of wide-to-narrow angle scatter, OSIR, throughout the subcellular compartment of living cells undergoing apoptosis or over-expressing BCL-x_L. The results showed that the OSIR decreased monotonically in the first 60 min of apoptosis to reach ~75% of its initial value. The early decrease in OSIR was reproducible in nontransfected CSM 14.1 cells and CSM 14.1 cells transfected with YFP. This decrease in OSIR occurred 5–6 h before membrane phosphatidyl serine exposure, and 9–10 h before loss of membrane integrity. Thus, the decrease in OSIR occurs very early on, at the onset of apoptosis. Preliminary data (not shown) from a BAX transfected CSM 14.1 line show that BAX, which is initially diffusely distributed within the cells, does not translocate to

the mitochondria 1 h after STS treatment. Evidence of BAX translocation starts appearing ~6–7 h after induction of apoptosis. As such, the changes in optical scattering might also well precede BAX translocation.

In apoptosis-resistant CSM 14.1 cells stably expressing YFP-BCL-x_L, there was little change in the light-scatter intensity ratio after STS treatment. However, the initial OSIR was already ~24% lower in the BCL-x_L cells compared with the YFP and nontransfected cells, suggesting that BCL-x_L cells start out with an altered OSIR baseline independently of the apoptosis stimulus. Thus, rather than ''blocking'' the decease in optical scatter ratio from a common baseline value, the overexpression of BCL-x_L on the mitochondria resulted in a drop in the starting value of the OSIR, such that the OSIR decreased by only 8.8% from its initial value in the BCL-x_L cells treated with 1 μM STS. This is compared to a 26% relative decrease in OSIR in nontransfected and 28% in YFP cell lines after treatment with 1 μM STS.

The change in OSIR must indicate changes in subcellular morphology, as changes in organelle geometry directly result in related changes in optical scattering (Fang et al., 2003). The scatter intensity ratio, OSIR, was experimentally shown to decrease monotonically with sphere diameter, $0.2\ \mu m < D < 1.5\ \mu m$, as predicted by theory (Boustany et al., 2001). In addition, numerical simulations of light scattering by spheres and ellipsoids showed that this scatter intensity ratio varies negligibly with changes in the refractive index (or composition) of the scattering particles (Boustany et al., 2002). Thus, if subcellular organelles were simply viewed as a collection of particles with an average characteristic diameter, a decrease in OSIR from 1.8 to 1.3 as observed for the untransfected cells in this study would correspond to an increase in this diameter length scale from 1.5 μm to 2.0 μm. This change in lengthscale provides a morphometric measure of cellular response. However, at present, the relationship between this average diameter lengthscale and the finer lengthscales of nonspherical, complex-shaped organelles still needs to be determined.

Although the cell cytoplasm may contain many several potential scatterers consisting of the different organelles, earlier results have shown that mitochondria should provide a very significant scattering signal (Beauvoit et al., 1995). Previously, we showed that an increase in the measured OSIR was correlated with mitochondrial rounding in response to an increase in intracellular calcium (Boustany et al., 2002). Those results corroborated the significance of the mitochondrial contribution to light scattering by cells. However, in this study, the changes in light scattering during apoptosis were not accompanied by large amplitude mitochondrial changes, such as the mitochondrial rounding observed earlier in response to calcium overload (Boustany et al., 2002). Here instead, obvious changes in mitochondrial morphology could not be resolved directly by DIC or fluorescence observation. Nevertheless, the fact that the initial value of the optical scatter ratio decreased as a result of overexpression of the mitochondria-bound BCL-x_L suggests that the scatter ratio involves mitochondrial alterations in the case of BCL-x_L overexpression. BCL-x_L, which is localized on the mitochondria may alter mitochondrial morphology, which in turn alters the angular scatter ratio measured by the OSIR. Initial alterations in light scattering due to the overexpression of mitochondria-bound BCL-x_L, even in the absence of staurosporine, also raise interesting questions as to the role of BCL-x_L in conferring apoptosis resistance by potentially preconditioning the cells before apoptosis induction.

We investigated whether the decrease in OSIR due to apoptosis and the OSIR initial decrease in baseline due to BCL-x_L overexpression could be due to the same subcellular events, since both decreases are comparable in magnitude. This could be the case if, for example, translocation of endogenous BCL-x_L to the mitochondria after initiation of apoptosis induced the observed OSIR decrease. In this scenario, the increased presence of BCL-x_L on the mitochondria due to either overexpression of BCL-x_L, or to BCL-x_L translocation after apoptosis induction would be the source of the OSIR decrease. Translocation of endogenous BCL-x_L from the cytoplasm to the mitochondria has previously been observed in murine thymocytes (Hsu et al., 1997) and kidney cells (Cuttle et al., 2001) and would support this hypothesis. Nonetheless, preliminary immunoblots of our nontransfected CSM 14.1 cell lines show that most of the endogenous BCL-x_L is bound to the subcellular membrane fraction of our cell lysates with very little BCL-x_L in the cytosolic fraction (data not shown). As such we could not reliably detect redistribution of endogenous BCL-x_L from the cytosol to the membrane fraction after STS treatment. The potential translocation of endogenous BCL- x_L from the cytosol to the membrane fraction of CSM14.1 cells remains to be tested.

In summary, this study demonstrates that staurosporine-induced apoptosis is accompanied by very early alterations in subcellular light scattering occurring within the first 60 min of staurosporine treatment, and well preceding the detection of typical early apoptosis markers, such as phosphatidyl serine exposure and possibly BAX translocation. The measured changes in OSIR could be used as a morphometric measure of cellular response at the onset of induced programmed cell death. Overexpression of mitochondria-bound BCL-x_L alters the optical scattering properties of CSM 14.1 cells, in addition to making them more resistant to apoptosis when compared with their YFP-transfected and nontransfected counterparts. This observation leads to the hypothesis that BCL-x_L-acquired apoptosis resistance involves initial mitochondrial morphological alterations, which cause in situ detectable changes in light scattering. The possibility of optically differentiating apoptosis-resistant cells from normal cells, or using light scattering to detect apoptosis may have important applications in anticancer drug development and cancer diagnosis. However, this prospect still depends on full elucidation of the relationship between light scattering, subcellular morphological alterations, expression of

antiapoptotic proteins such as BCL-x_L, and cell resistance to apoptosis.

This work was supported by National Institutes of Health grant R21-RR15264.

REFERENCES

Beauvoit, B., S. M. Evans, T. W. Jenkins, E. E. Miller, and B. Chance. 1995. Correlation between the light scattering and the mitochondrial content of normal tissues and transplantable rodent tumors. *Anal. Biochem.* 226:167–174.

Boustany, N. N., R. Drezek, and N. V. Thakor. 2002. Calcium-induced alterations in mitochondrial morphology quantified in situ with optical scatter imaging. *Biophys. J.* 83:1692–1700.

Boustany, N. N., S. C. Kuo, and N. V. Thakor. 2001. Optical scatter imaging: subcellular morphometry in situ with Fourier filtering. *Opt. Lett.* 26:1063–1065.

Camilleri-Broet, S., H. Vanderwerff, E. Caldwell, and D. Hockenbery. 1998. Distinct alterations in mitochondrial mass and function characterize different models of apoptosis. *Exp. Cell Res.* 239:277–292.

Cuttle, L., X.-J. Zhang, Z. H. Endre, C. Winterford, and G. C. Gobe. 2001. Bcl-X_L translocation in renal tubular epithelial cells in vitro protects distal cells from oxidative stress. *Kidney Int.* 59:1779–1788.

Desagher, S., and J. C. Martinou. 2000. Mitochondria as the central control point of apoptosis. *Trends Cell Biol.* 10:369–377.

Fang, H., M. Ollero, E. Vitkin, L. M. Kimerer, P. B. Cipolloni, M. M. Zaman, S. D. Freedman, I. J. Bigio, I. Itzkan, E. B. Hanlon, and L. T. Perelman. 2003. Noninvasive sizing of subcellular organelles with light scattering spectroscopy. *IEE Journal of Selected Topics in Quantum Electronics*. 9:267–276.

Finucane, D. M., E. Bossy-Wetzel, N. J. Waterhouse, T. G. Cotter, and D. R. Green. 1999. Bax-induced caspase activation and apoptosis via cytochrome c release from mitochondria is inhibitable by Bcl-xL. *J. Biol. Chem.* 274:2225–2233.

Frank, S., B. Gaume, E. S. Bergmann-Leitner, W. W. Leitner, E. G. Robert, F. Catez, C. L. Smith, and R. J. Youle. 2001. The role of dynamin-related protein 1, a mediator of mitochondrial fission, in apoptosis. *Dev. Cell.* 1:515–525.

Gross, A., J. M. McDonnall, and S. J. Korsmeyer. 1999. Bcl-2 family members and the mitochondria in apoptosis. *Genes Dev.* 13:1899–1911.

Hsu, Y.-T., K. G. Wolter, and R. J. Youle. 1997. Cytosol-to-membrane resdistribution of Bax and Bcl-X_L during apoptosis. *Proc. Natl. Acad. Sci. USA.* 94:3668–3672.

Jurgensmeier, J. M., Z. Xie, Q. Deveraux, L. Ellerby, D. Bredesen, and J. C. Reed. 1998. Bax directly induces release of cytochrome c from isolated mitochondria. *Proc. Natl. Acad. Sci. USA.* 95:4997–5002.

Kowaltowski, A. J., R. G. Cosso, C. B. Campos, and G. Fiskum. 2002. Effect of Bcl-2 overexpression on mitochondrial structure and function. *J. Biol. Chem.* 277:42802–42807.

Mancini, M., B. O. Anderson, E. Caldwell, M. Sedghinasab, P. B. Paty, and D. M. Hockenbery. 1997. Mitochondrial proliferation and paradoxical membrane depolarization during terminal differentiation and apoptosis in a human colon carcinoma cell line. *J. Cell Biol.* 138:449–469.

Martinou, I., S. Desagher, R. Eskes, B. Antonsson, E. Andre, S. Fakan, and J.-C. Martinou. 1999. The release of cytochrome c from mitochondria during apoptosis of NGF-deprived sympathetic neurons is a reversible event. *J. Cell Biol.* 144:883–889.

Mootha, V. K., M. C. Wei, K. F. Buttle, L. Scorrano, V. Panoutsakopoulou, C. A. Mannella, and S. J. Korsmeyer. 2001. A reversible component of mitochondrial respiratory dysfunction in apoptosis can be rescued by exogenous cytochrome c. *EMBO J.* 20:661–671.

Narita, M., S. Shimizu, T. Ito, T. Chittenden, R. J. Lutz, H. Matsuda, and Y. Tsujimoto. 1998. Bax interacts with the permeability transition pore to induce permeability transition and cytochrome c release in isolated mitochondria. *Proc. Natl. Acad. Sci. USA.* 95:14681–14686.

Ott, M., J. D. Robertson, V. Gogvadze, B. Zhivotovsky, and S. Orrenius. 2002. Cytochrome c release from mitochondria proceeds by a two-step process. *Proc. Natl. Acad. Sci. USA.* 99:1259–1263.

Reipert, S., J. Berry, M. Hughes, J. A. Hickman, and T. D. Allen. 1995. Changes of mitochondrial mass in the hemopoietic stem cell line FDCP-mix after treatment with etoposide: a correlative study by multiparameter flow cytometry and confocal and electron microscopy. *Exp. Cell Res.* 221:281–288.

Scorrano, L., M. Ashiya, K. Buttle, S. Weiler, S. A. Oakes, C. A. Mannella, and S. J. Korsmeyer. 2002. A distinct pathway remodels mitochondrial cristae and mobilizes cytochrome c during apoptosis. *Dev. Cell.* 2:55–67.

Vander-Heiden, M. G., N. S. Chandel, E. K. Williamson, P. T. Schumacker, and C. B. Thompson. 1997. Bcl-xL regulates the membrane potential and volume homeostasis of mitochondria. *Cell.* 91:627–637.

von Ahsen, O., C. Renken, G. Perkins, R. M. Kluck, E. Bossy-Wetzel, and D. D. Newmeyer. 2000. Preservation of mitochondrial structure and function after Bid- or Bax-mediated cytochrome c release. *J. Cell Biol.* 150:1027–1036.

Zamzami, N., S. A. Susin, P. Marchetti, T. Hirsch, I. Gomez-Monterrey, M. Castedo, and G. Kroemer. 1996. Mitochondrial control of nuclear apoptosis. *J. Exp. Med.* 183:1533–1544.